Conf-830772--2

IMPLICATIONS OF HEAVY-ION-INDUCED SATELLITE X-RAY EMISSION. I*

Introduction

CONF-830772--2

DE83 015682

S. RAMAN and C. R. VANE

Oak Ridge National Laboratory, Oak Ridge, Tennessee 37830 USA

IMPLICATIONS OF HEAVY-ION INDUCED SATELLITE X-RAY EMISSION I*

Introduction

S. RAMAN and C. R. VANE

Oak Ridge National Laboratory, Oak Ridge, Tennessee 37830 USA

Regardless of how they are induced, X-ray spectra are sensitive to the chemical environment of the emitting atom and can yield information on the atomic and electronic structure of host materials. Those spectra resulting from light ion and heavy ion excitations are the main topics covered in this series of papers. Highly energetic heavy ions are capable of producing multiple inner-shell ionization. The resulting spectrum of X-rays from a particular target atom is composed of a complex series of satellite lines. Environmental effects give rise to the redistribution of intensity from one satellite group to another. These changes can be correlated with bulk chemical properties (valence electron densities, effective charges, covalencies, etc.). The possibility of obtaining new chemical information (for example, in implanted materials and in metal alloys) exists but requires greater experimental and theoretical understanding of both parametric variations and the fine structure of satellite lines.

*Research sponsored by the Division of Basic Energy Sciences, U.S. Department of Energy, under Contract No. W-7405-eng-26 with the Union Carbide Corporation. Accordingly, the U.S. government retains a nonexclusive, royalty-free license to publish or reproduce the published form of this contribution, or allow others to do so, for U.S. government purposes.

1. Introduction

The excitation of X-ray satellites by fast heavy ions and the effects of chemical environment on the relative intensities of X-ray satellites are the basic topics treated in the present series of papers. Paper I serves both as a broad introduction to the subject and as a guide to the subsequent papers in this series (referred to as Paper II, Paper III, etc.). For delving further into these topics, the reader will find several recent books [1-3] of great utility. A review article [4] deals specifically with ion-induced X-ray spectroscopy.

2. X-ray yields

The detailed study of K_α satellite spectra discussed in the next section requires the use of a high-resolution crystal spectrometer because the energy differences between adjacent peaks are quite small (~ 17 eV for S). Such spectrometers generally possess low efficiencies. In order to arrive at reliable estimates for the expected count rates, it is necessary to resort to experimental X-ray production data [5,6], or, failing to find such data, to resort to theory [5,6]. Experimental data for energetic (> 1 MeV/u) heavy ions are more sparse than generally believed. Theories do exist for adequately describing inner-shell ionization induced by light ions but their applicability to heavy ions is seriously open to question. To complicate matters further, calculated cross sections pertain to vanishingly thin targets [7,8] and such cross sections depend strongly on the charge state of the projectile [9]. In studying chemical effects, relatively thick solid targets are the norm and solid target X-ray studies measure only the effects of an equilibrium charge distribu-

tion. Fortunately, the cross sections and X-ray yields from solid targets due to heavy ion impact are large enough that they can be readily measured for the selected ion-target combination with a Si(Li) or Ge(Li) X-ray detector. Our attempts to measure X-ray production induced by energic Ar ions from V, Cu, Nb, Ta, and Pt targets and comparisons with theory are described in Paper II.

3. Satellite peaks

The measurement of X-ray spectra produced by ion bombardment shows that multiple ionization is present in high-energy collisions [10-12]. The first peak in fig. 1 is composed of the usual K_{α_1} and K_{α_2} lines whereas the peaks which follow are satellite peaks composed of K_α X-rays arising from configurations having n (one, two, ...) L-shell vacancies. The energies of the satellite peaks are consistent with Hartree-Fock-Slater calculations for multiply ionized atoms [10,11,13,14]. The peaks are in general complex; the $K_\alpha{}^1L^1$ peak contains five transition lines, the $K_\alpha{}^1L^4$ peak over twenty.

The use of a binomial distribution of probabilities has been suggested [15,16] for treating spectra of the type shown in fig. 1. This distribution assumes independent production of outer shell (L) vacancies. If f_n denotes the fractional intensity of the nth satellite peak, the apparent L-vacancy fraction is defined as

$$p_L = \frac{1}{N} \sum_n n f_n \qquad (1)$$

where N is the number of L-shell electrons in the ground state. This p_L value can also be inserted in the approximate expression

$$f_n \approx \binom{N}{n} (p_L)^n (1 - p_L)^{N-n} (\omega_n/\bar{\omega}) \qquad (2)$$

where $\overline{\omega}$ is the total mean fluorescence yield, ω_n the average fluorescence yield for the nth charge state, and

$$\binom{N}{n} = N!/(N-n)!n!. \qquad (3)$$

The binomial probability parameter p_L may be interpreted approximately as the average L-shell ionization probability per electron for K-shell ionizing collisions [14]. A strict binomial distribution describes light-ion induced X-ray spectra fairly well [17] but not heavy-ion induced spectra (see fig. 2) especially in solids [17,18]. The reason is primarily that the fluorescence yield does vary ($\omega_n/\overline{\omega} \neq 1$) depending on the degree of ionization as well as on the particular configuration of the state and because the possibility of outer vacancy refilling is not taken into account. Nevertheless, p_L is a convenient parameter to describe the data; p_L values increase rapidly with increasing projectile atomic number (Z_1), reach a maximum near $Z_1 \approx Z_2$ where Z_2 is the target atomic number, and decrease slightly thereafter [14]. The p_L values (and the absolute cross sections for satellite production) have been calculated from theory [17,19] but the agreement between experiment and theory, especially for heavy-ion projectiles, is poor. There also exist in the literature universal curves for appropriately scaled experimental p_L values [20,21] and p_M values [22] versus a scaled projectile velocity.

The p_L values for NaSCN and Na_2SO_4 are quite different because the spectra (see fig. 1) are different. Higher p_L values imply that the higher energy satellite peaks are enhanced. At high bombarding energies (projectile velocity >> orbital electron velocity), the initial L-vacancy distributions generated at the time of collision are not expected to depend significantly on the chemical

environment. The observed differences should then be attributable to a fast vacancy rearrangement prior to K_α X-ray emission. Such massive rearrangements could occur via electron transfer from the shells further out than L (intra-atomic transitions) or from the neighboring atoms (interatomic transitions). Of these two, interatomic transitions appear to be dominant [23,24], and cause spectra from different chemical compounds to be different.

A major uncertainty in specifying the extent of rearrangement is the determination of M-shell population which can at best be inferred from energy shifts. To study the M-shell ionization and rearrangement, several authors [25-27] have resorted to relatively simple and isolated systems. Comparisons of the spectra of a variety of gaseous and solid compounds support the conclusion that interatomic M→M electron transfer with subsequent intra-atomic M→L and M→K decay as well as direct interatomic M→L transfer dominate the fast rearrangement occurring prior to K_α X-ray emission in atoms having highly depleted M shells.

4. Chemical effects

It is interesting to note that in one of the earliest reported attempts to discern differences in heavy-ion induced X-ray satellite spectra from different chemical species, the K_α spectra from Al metal and Al_2O_3 due to 5-MeV ^4He impact were in fact strikingly similar [13]. However, in the next set of compounds which were studied and reported (32-MeV ^{16}O ions on sulfur compounds), marked changes were indeed observed in the intensity distribution of satellite lines [23]. Our studies of sulfur compounds are described in Paper III. The apparent lack of sensitivity in the Al case has since been confirmed [24] but not yet satisfactorily explained.

The environmental effects on the intense K_α and L_α satellite structure produced by heavy-ion bombardment have been studied by several authors. As shown in table 1, a comprehensive body of high-resolution (crystal spectrometer) information exists for a variety of collision partners at a wide range of relative velocities.

Empirical observations (see references cited in table 1) show that both energies and widths of core levels in atoms bound in molecular systems are influenced by the chemical state and ligand environment of the emitting atom. In the case of third row elements, the valence electrons are in the M shell. The chemical effects are directly attributable to the influence of chemical bonding on the rates of K→M and L→M vacancy transfer processes. It is to be expected that the rates of electron transitions from the M shell to the L shell will depend quite sensitively on the valence electron density, which in turn is influenced by chemical bonding. Because the Auger rates involving the M electrons are affected, the fluorescence yields corresponding to each of the individual satellite peaks will also depend on the chemical bonding.

The sharing of electrons in strong bonds among molecules essentially determines the structure of interest in the X-ray spectroscopy. The valence electron localization increases in going from the metallic through covalent to ionic bonding [3]. In ionic compounds, the electrons are localized in one of the atoms, in covalent compounds between the atoms, and in metals throughout the lattice.

The effective charge q on an ion A in a molecule can be expressed [3] as

$$q_{eff} = \sum_{\mu} \{1 - \exp[-0.25(X_A - X_B)^2]\}_{\mu} \qquad (4)$$

where X denotes the electronegativity and the sum is over the bonds that connect ion A with the different neighbors B. The effective charge is a measure of the local valence electron density.

Another quantity, the average total valence electron density of a compound is given by

$$D_V = 0.602 \frac{n_V \rho}{W_{mol}} \text{ electrons/Å}^3, \qquad (5)$$

where n_V is the total number of valence electrons, ρ is the mass density, and W_{mol} is the molecular weight.

In the case of Al, Si, S, and Cl compounds, the p_L values decrease with the effective charge [24,27]. This behavior for S compounds is shown in fig. 3. If localized electrons and no others participate in the rearrangement, this behavior is exactly opposite to that expected. Therefore, the conclusion must be that the localized valence electrons are ionized during the collision. At the same time, the p_L values decrease with increasing average total valence electron density (see fig. 3). This is strong evidence that valence electrons from neighboring atoms rush to neutralize the target atom which has just ejected a single K-shell electron, several L-shell electrons, and nearly all valence M-shell electrons as a result of an energetic heavy-ion collision.

Whereas previous authors have found p_L values derived from all satellite peaks [see eq. (1)] to be useful in representing the data and in correlating with chemical properties, we have found that the fractional area f_5 of the K^1L^5 peak by itself correlates well with D_V and the area f_2 of the K^1L^2 peak with q_{eff} (see Paper III).

An intercomparative study [29,39,40] of fluorine K_α X-ray satellites produced by photon, electron, ^4He, ^{12}C, and ^{14}N impacts also shows that the primary vacancy distributions in fluorine compounds are altered by interatomic electronic transitions prior to K_α X-ray emission. The fluorine L-vacancy filling rate was found to increase linearly with the covalency, implying that the interatomic transitions proceed mainly through a covalent component in the molecular orbital in the fluorides [39]. Recent measurements on alkali-metal and alkaline-earth fluoride components have shown that a resonant transfer of electrons from neighboring atoms can occur when level-matching conditions exist [32,33,40].

In order to be useful for applications, the p_L values for different compounds of a particular element must be distinguishable. With 2 MeV/u ^{16}O projectiles, the variation in p_L is 4% in Al compounds, 6% in Cl compounds, 10% in Si compounds, and 18% in S compounds [27]. Based on 2 MeV/u O, Ne, and Ar projectiles, it was once believed [41] that a greater variation in p_L values might be achievable with heavier projectiles such as Kr. Figure 3 shows that these expectations are not borne out. The explanation is that the p_L values tend to saturate with large Z_1 [42]. Changing projectile velocity does not help either; sulfur K_α satellites generated by 6 MeV/u ^{14}N ions show no significant chemical effect [34].

With 6 MeV/u $^{14}N^{4+}$ projectiles, no significant chemical effects were seen [34] for compounds of $9<Z<30$ except for F ($Z=9$) and Na ($Z=11$). Striking chemical effects have been observed, on the other hand, for fluorine compounds not only with 6 MeV/u ^{14}N [34], but also with a wide variety of light and heavy ions at different projectile energies (see table 1), with ≈ 6 keV electrons [43], and even with 20 keV photons [43]. The mean K-hole lifetime is presumably longer in F ($\sim 10^{-13}$ sec) than in S ($\sim 10^{-15}$ sec).

The L X-ray satellite spectra emitted from 3d transition elements also show intensity variations when excited by heavy ions [37]. It is evident from fig. 4 that unlike the K X-ray case information is more difficult to extract due to the superposition of a prohibitively large number of lines. Attempts to study and interpret spectral difference in L X-ray spectra from Mo compounds, alloys, and intermetallic compounds are discussed in Paper IV.

Even the K_α X-ray satellite lines can be studied more profitably with superior resolution. The analysis of such data until now has been in terms of the fractional area of a particular satellite peak. When the K^1L^5 line of sulfur is studied with ~ 1 eV resolution, striking differences are observed as shown in fig. 5. Our high-resolution measurements are discussed in Paper V.

5. Applications

In dealing with heavy-ion induced satellite X-ray emission in solids, a basic and thorough understanding of the underlying physical phenomena has been so lacking that despite the numerous observations that have been made (see table 1) on spectral variations from compound to compound, concrete examples of important practical problems solved by this novel technique have been equally lacking.

The potential for applications does exist. For example, in a controlled experiment [30], 50 keV F^- ions were implanted in Fe at fluence levels calculated to produce FeF_3. Subsequently, 2-MeV ^4He ions were employed to show that the implanted structure was indeed FeF_3. Had the F ions simply entered the Fe lattice, the satellite spectrum would have been typical of ionic binding and resembled the NaF spectrum, which it did not.

The K_α satellite intensities (represented by p_L) depend on projectile energy and therefore reflect the energy loss suffered by an ion as a result of passing through a surface layer. This fact has been exploited to determine the thicknesses of C and Al layers on the surfaces of thick Si substrates [44]. The precision of this method is approximately ± 18 $\mu g/cm^2$ for Al layers ranging in thickness from 0 to 600 $\mu g/cm^2$, and ± 32 $\mu g/cm^2$ for C layers from 0 to 1500 $\mu g/cm^2$. Further improvements in precision could come from a judicious choice of projectile energy and velocity.

5. Summary

Heavy ions produce X-ray satellites not observed with other means of excitation. The satellite intensity distributions reveal a dependence on chemical environment. These variations can be empirically correlated with bulk chemical properties. The chemical sensitivity arises from interatomic electron transfer and fast rearrangement occurring prior to X-ray emission. The results of studies conducted thus far provide a glimpse of the wealth of information concerning relaxation processes for highly ionized atoms obtainable from ion-excited X-ray satellite spectra. Further experimental work (with a variety of projectiles of different energies on many more compounds studied with superior resolution) appears desirable in order to obtain a better understanding of the basic physical phenomena. There is also an acute need for extended theoretical treatments incorporating both solid state and multiple ionization effects.

Acknowledgments

[1] Atomic Inner-Shell Processes, vols. I and II, ed. B. Crasemann (Academic Press, New York, 1975).

[2] Atomic Physics: Accelerators, ed. P. Richard (Academic Press, New York, 1980).

[3] B. K. Agarwal, X-Ray Spectroscopy (Springer-Verlag, Berlin, 1979).

[4] F. Hopkins, in ref. [2], p. 355.

[5] J. D. Garcia, R. J. Fortner, and T. M. Kavanagh, Rev. Mod. Phys. 45 (1973) 111.

[6] Eleven compilations on measurements and calculations of inner-shell ionization have appeared. See Inner-Shell Ionization, Cumulated Subject Index, At. Data Nucl. Data Tables, ed. K. Way, 27 (1982) 627.

[7] R. K. Gardner, T. J. Gray, P. Richard, C. Schmiedekamp, K. A. Jamison, and J. M. Hall, Phys. Rev. A 15 (1977) 2202.

[8] T. J. Gray, P. Richard, G. Gealy, and J. Newcomb, Phys. Rev. A 19 (1979) 1424.

[9] J. R. McDonald, in ref. [2], p. 279.

[10] A. R. Knudson, D. J. Nagel, P. G. Burkhalter, and K. L. Dunning, Phys. Rev. Lett. 26 (1971) 1149.

[11] D. Burch, P. Richard, and R. L. Blake, Phys. Rev. Lett. 26 (1971) 1355.

[12] C. F. Moore, M. Senglaub, B. Johnson, and P. Richard, Phys. Lett. 40A (1972) 107.

[13] P. G. Burkhalter, A. R. Knudson, D. J. Nagel, and K. L. Dunning, Phys. Rev. A 6 (1972) 2093.

[14] R. L. Watson, F. E. Jenson, and T. Chiao, Phys. Rev. A 10 (1974) 1230.

[15] D. Burch and H. Swanson, Proc. Int. Conf. Inner-Shell Ionization Phenomena, Atlanta (1972), eds. R. F. Fink, S. T. Manson, J. M. Palms, and P. V. Rao, USAEC CONF-720404 (1973) 1464.

[16] J. M. Hansteen and O. P. Mosebekk, Phys. Rev. Lett. 29 (1972) 1361.

[17] R. L. Kauffman, J. H. McGuire, P. Richard, and C. F. Moore, Phys. Rev. A 8 (1973) 1233.

[18] R. J. Fortner and D. L. Mathews, Phys. Rev. A 14 (1976) 2357.

[19] J. H. McGuire and P. Richard, Phys. Rev. A 8 (1973) 1374.

[20] C. Schmiedekamp, B. L. Doyle, T. J. Gray, R. K. Gardner, K. A. Jamison, and P. Richard, Phys. Rev. A 18 (1978) 1892.

[21] R. L. Watson, B. I. Sonobe, J. A. Demarest, and A. Langenberg, Phys. Rev. A 19 (1979) 1529.

[22] Y Awaya, Electronic and Atomic Collisions, eds. N. Oda and K. Takayanagi (North-Holland, Amsterdam 1980) p. 325.

[23] R. L. Watson, T. Chiao, and F. E. Jenson, Phys. Rev. Lett. 35 (1975) 254.

[24] R. L. Watson, A. K. Leeper, B. I. Sonobe, T. Chiao, and F. E. Jenson, Phys. Rev. A 15 (1977) 914.

[25] R. L. Kauffman, K. A. Jamison, T. J. Gray, and P. Richard, Phys. Rev. Lett. 36 (1976) 1074.

[26] F. Hopkins, A. Little, N. Cue, and V. Dutkiewicz, Phys. Rev. Lett. 37 (1976) 1100.

[27] J. A. Demarest and R. L. Watson, Phys. Rev. A 17 (1978) 1302.

[28] G. Deconninck, Z. Szökefalvi-Nagy, and S. Van Den Broek, Proc. Intern. Conf. X-Ray and XUV Spectroscopy, Japanese J. App. Phys. 17, Supplement 17-2 (1978) 357.

[29] M. Uda, H. Endo, K. Maeda, Y. Sasa, and M. Kobayashi, Z. Phys. A 300 (1981) 1.

[30] G. Deconninck and S. Van Den Broek, J. Phys. C 13 (1980) 3329.

[31] G. Deconninck and S. Van Den Broek, 1980 Conf. Application of Accelerators in Research and Industry, eds. J. L. Duggan and I. L. Morgan, IEEE Trans.

Nucl. Sci. NS-28 (1981) 1404; Inner-Shell and X-Ray Physics of Atoms and Solids, eds., D. J. Fabian and H. Kleinpoppen, and L. M. Watson (Plenum, New York, 1981) p. 811.

[32] O. Benka, R. L. Watson, and R. A. Kenefick, Phys. Rev. Lett. 47 (1981) 1202.

[33] O. Benka, R. L. Watson, K. Parthasaradhi, J. M. Sanders, and R. J. Maurer, Phys. Rev. A 27 (1983) 149.

[34] H. Endo and M. Uda, Z. Phys. A 306 (1982) 187. See also [39].

[35] C. R. Vane et al., Paper III in this series.

[36] T. M. Rosseel et al., unpublished results.

[37] M. Uda, K. Maeda, H. Endo, Y. Sasa, and M. Kobayashi, Inner-Shell and X-Ray Physics of Atoms and Solids, eds., D. J. Fabian, H. Kleinpoppen, and L. M. Watson (Plenum, New York, 1981) p. 205.

[38] T. M. Rosseel et al., Paper IV in this series.

[39] M. Uda, H. Endo, K. Maeda, Y. Awaya, M. Kobayashi, Y. Sasa, H. Kumagi, and T. Tonuma, Phys. Rev. Lett. 42 (1979) 1257.

[40] R. L. Watson, O. Benka, K. Parthasaradhi, R. A. Kenefick, R. J. Maurer, J. M. Sanders, B. Bandong, and T. Ritter, 1982 Conf. Application of Accelerators in Research and Industry, eds. J. L. Duggan and I. L. Morgan, IEEE Trans. Nucl. Sci. NS-30 (1983) 919.

[41] R. L. Watson, J. A. Demarest, A. Langenberg, F. E. Jenson, J. R. White, and C. C. Bahr, 1978 Conf. Application of Accelerators in Research and Industry, eds. J. L. Duggan and I. L. Morgan, IEEE Trans. Nucl. Sci. NS-26 (1979) 1352.

[42] R. L. Becker, A. L. Ford, and J. F. Reading, in these Proceedings.

[43] H. Endo, M. Uda, and K. Maeda, Phys. Rev. A 22 (1980) 1436.

[44] R. L. Watson, A. K. Leeper, and B. I. Sonobe, Nucl. Instr. and Meth. 142 (1977) 311.

Table 1. Summary of studies involving satellite lines induced by light and heavy ions from two or more compounds of a particular element. X-rays other than $K_\alpha{}^1L^n$ and $L_\alpha{}^{1,2}M^m$ are not included.

Ion	Energy (MeV/u)	Targets	X-rays	Ref.
^1H	1.5	MgO, CaO, ZnO, BaO, SiO_2, TiO_2, MnO_2, CeO_2, Al_2O_3, Ca_2O_3, Cr_2O_3, Ni_2O_3	O $K_\alpha{}^1L^n$	[28]
^4He	1-2	MgO, CaO, BaO, SiO_2, MnO_2, Al_2O_3, Ca_2O_3, Cr_2O_3, Ni_2O_3	O $K_\alpha{}^1L^n$	[28]
^1H	1.5	NaF, BaF_2, $(CF_2)_n$, $(CHF\text{-}CF_2)_n$, $(CH_2\text{-}CF_2)_n$	F $K_\alpha{}^1L^n$	[28]
^4He	2.0	NaF, BaF_2, $(CF_2)_n$	F $K_\alpha{}^1L^n$	[28]
^1H	6.0	NaF, Na_3AlF_6, AlF_3, NiF_2, CuF_2, $(CF_2)_n$	F $K_\alpha{}^1L^n$	[29]
^4H	0.5	LiF, NaF, KF, MgF_2, CaF_2, SrF_2, BaF_2, FeF_3, Na_2PO_3F, $(CF_2)_n$, $(CH_2\text{-}CF_2)_n$	F $K_\alpha{}^1L^n$	[30]
^4He	0.5	LiF, NaF, KF, RbF, AgF, CsF, BeF_2, MgF_2, CaF_2, CrF_2, FeF_2, CoF_2, NiF_2, CuF_2, ZnF_2, SnF_2, BaF_2, PbF_2, AlF_3, TiF_3, FeF_3, SbF_3, TiF_4, SnF_4	F $K_\alpha{}^1L^n$	[31]
^4He	1.4	NaF, KF, RbF, CsF, MgF_2, CaF_2, SrF_2, BaF_2	F $K_\alpha{}^1L^n$	[32]
^4He	6.0	NaF, Na_3AlF_6, AlF_3, NiF_2, CuF_2, $(CF_2)_n$	F $K_\alpha{}^1L^n$	[29]
^{12}C	1.8	LiF, NaF, KF, RbF, MgF_2, CaF_2, SrF_2, BaF_2	F $K_\alpha{}^1L^n$	[33]
^{12}C	6.0	NaF, Na_3AlF_6, AlF_3, NiF_2, CuF_2, $(CF_2)_n$	F $K_\alpha{}^1Ln$	[29]
^{14}N	6.0	NaF, Na_3AlF_6, AlF_3, NiF_2, CuF_2, $(CF_2)_n$	F $K_\alpha{}^1L^n$	[34]
^4He	0.5	NaF, NaCl, NaBr	Na $K_\alpha{}^1L^n$	[30]
^{14}N	6.0	NaF, Na_3AlF_6, Na_2SO_4, NaSCN, $Na_2S_2O_6$	Na $K_\alpha{}^1L^n$	[34]
^{14}N	6.0	MgO, MgF_2	Mg $K_\alpha{}^1L^n$	[34]
^4He	1.25	Al, AlN, Al_2O_3	Al $K_\alpha{}^1L^n$	[13]
^{16}O	2.0	Al, AlB_2, Al_4C_3, Al_2O_3, AlN, AlSi, Al_2S_3	Al $K_\alpha{}^1L^n$	[24]

Ion	Energy (MeV/u)	Targets	X-rays	Ref.
^{20}Ne	0.25	Al, AlN, Al_2O_3	Al $K_\alpha^1L^n$	[13]
^{4}He	1.2	Si, SiH_4	Si $K_\alpha^1L^n$	[21]
^{4}He	1.4	Si, SiO, SiO_2	Si $K_\alpha^1L^n$	[24]
^{12}C	1.8	Si, SiO, SiO_2	Si $K_\alpha^1L^n$	[24]
^{16}O	2.0	AlSi, Si, SiB_6, SiC, Si_3N_4, SiO, SiO_2	Si $K_\alpha^1L^n$	[24]
^{16}O	2.0	Si, SiH_4, SiF_4	Si $K_\alpha^1L^n$	[27]
^{35}Cl	1.3	Si, SiH_4	Si $K_\alpha^1L^n$	[25]
^{35}Cl	1.5	SiH_4, SiF_4	Si $K_\alpha^1L^n$	[26]
^{4}He	1.2	S_8, H_2S, SF_6	S $K_\alpha^1L^n$	[21]
^{14}N	6.0	Na_2SO_4, Cu_2S	S $K_\alpha^1L^n$	[34]
^{16}O	2.0	S_8, $(NH_4)_2SO_4$, Na_2S, Na_2SO_3, Na_2SO_4, Al_2S_3, FeS, ZnS, CdS	S $K_\alpha^1L^n$	[24]
^{16}O	2.0	S_8, H_2S, SO_2, SF_6	S $K_\alpha^1L^n$	[27]
^{20}Ne	2.0	S_8, Na_2S, Na_2SO_4	S $K_\alpha^1L^n$	[24]
^{35}Cl	1.5	H_2S, SF_6	S $K_\alpha^1L^n$	[26]
^{40}Ar	0.9	S_8, Na_2S, Na_2SO_3, Na_2SO_4, $Na_2SO_2O_3$, $NaHSO_3$, NaScN, MnS, FeS, FeS_2, CoS, ZnS	S $K_\alpha^1L^n$	[35]
^{40}Ar	2.0	S_8, Na_2S, Na_2SO_4	S $K_\alpha^1L^n$	[24]
^{80}Kr	1.0	Na_2SO_4, NaSCN	S $K_\alpha^1L^n$	[35]
^{2}H	1.7	NaCl, KCl	Cl $K_\alpha^1L^n$	[14]
^{4}He	1.2	HCl, KCl	Cl $K_\alpha^1L^n$	[21]
^{4}He	1.7	NaCl, KCl	Cl $K_\alpha^1L^n$	[14]
^{12}C	1.8	NaCl, KCl	Cl $K_\alpha^1L^n$	[14]
^{14}N	6.0	NaCl, KCl	Cl $K_\alpha^1L^n$	[34]

Ion	Energy (MeV/u)	Targets	X-rays	Ref.
^{16}O	2.0	NaCl, KCl	Cl $K_\alpha{}^1L^n$	[14]
^{16}O	2.0	Cl_2, HCl, CCl_4, CaCl, KCl	Cl $K_\alpha{}^1L^n$	[27]
^{16}O	2.0	LiCl, $BeCl_2$, NH_4Cl, NaCl, $MgCl_2$, KCl, $CaCl_2$, $MnCl_2$, $NiCl_2$, $ZnCl_2$, RbCl, $SrCl_2$, CsCl, $BaCl_2$	Cl $K_\alpha{}^1L^n$	[24]
^{20}Ne	2.0	NaCl, KCl	Cl $K_\alpha{}^1L^n$	[14]
^{32}S	2.0	NaCl, KCl	Cl $K_\alpha{}^1L^n$	[14]
^{40}Ar	2.0	NaCl, KCl	Cl $K_\alpha{}^1L^n$	[14]
^{35}Cl	1.03	Ti, TiO_2, Ti_2O_3, $TiSi_2$, Ti_3Mo, TiMo, $TiMO_3$	Ti $K_\alpha{}^1L^n$	[36]
^{14}N	6.0	V, VF_3	V $K_\alpha{}^1L^n$	[34]
^{35}Cl	1.03	V, VC, V_2O_5, VSi_2, VS, $V(Ni_{0.57}Co_{0.43})_3$, $V(Fe_{0.22}Co_{0.78})_3$, $V(Fe_{0.5}Ni_{0.5})_3$, $V(Fe_{0.40}Ni_{0.10}Co_{0.50})_3$, $V(Fe_{0.33}Co_{0.67})_3$	V $K_\alpha{}^1L^n$	[36]
^{14}N	6.0	Mn, MnF_2	Mn $K_\alpha{}^1L^n$	[34]
^{14}N	6.0	Fe, Fe_2O_3, FeF_3	Fe $K_\alpha{}^1L^n$	[34]
^{14}N	6.0	Co, CoF_3	Co $K_\alpha{}^1L^n$	[34]
^{14}N	6.0	Ni, NiF_2	Ni $K_\alpha{}^1L^n$	[34]
^{14}N	6.0	Cu, CuF_2	Cu $K_\alpha{}^1L^n$	[34]
^{14}N	6.0	CuO, Cu_2O, CuF_2	Cu $L_\alpha{}^1M^m$	[37]
^{14}N	6.0	Fe, FeO, Fe_2O_3, FeF_3	Fe $L_\alpha{}^1M^m$	[37]
^{13}N	6.0	Ni, NiO, NiF_2	Ni $L_\alpha{}^1M^m$	[37]
^{14}N	6.0	Zn, ZnO, ZnF_2	Zn $L_\alpha{}^1M^m$	[37]
^{14}N	6.0	Ge, GeO_2	Ge $L_\alpha{}^1M^m$	[37]
^{35}Cl	1.03	Mo, Mo_2C, MoO_2, MoO_3, $MoSi_2$, Mo_3Ti, MoTi, $MoTi_3$, $MoSe_2$, $MoTe_2$, $MoIr_3$, Mo_3Ir	Mo $L_\alpha{}^2M^m$	[38]

Fig. 1. Single-crystal spectrometer measurements of S K_α X-rays produced by 36-MeV Ar projectiles.

Fig. 2. Relative intensity ratios for S satellites produced by 36-MeV Ar projectiles. The hatched bars are the measured ratios. The light bars are the values obtained by fitting the data to a binomial distribution ratner than by using eq. (1).

Fig. 3. Variation of p_L with average valence electron density and with effective charge.

Fig. 4. Single-crystal spectrometer measurements of Mo L X-rays produced by 36-MeV ^{35}Cl projectiles.

Fig. 5. High-resolution measurements of the S K^1L^5 peak (one K-shell hole and five L-shell holes) induced by 34-MeV ^{35}Cl projectiles.

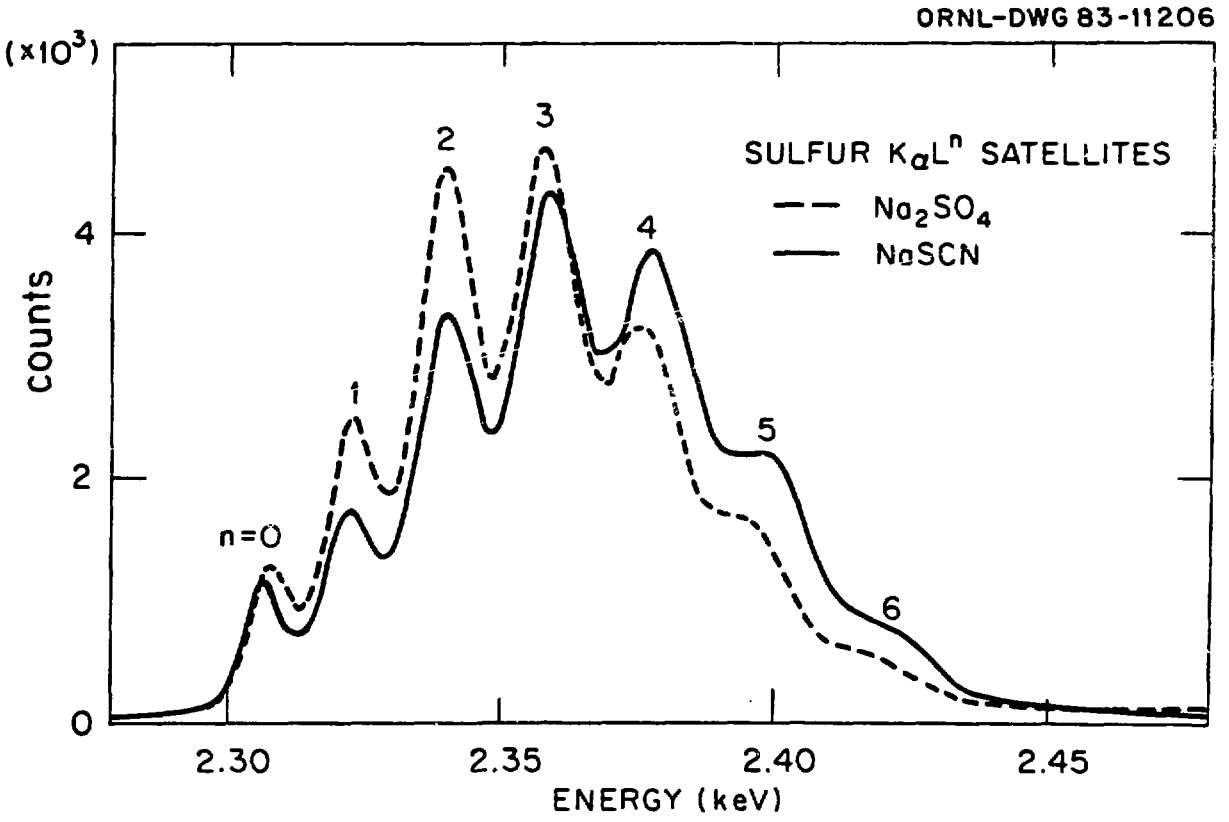
ORNL-DWG 83-11206
(x10³)
counts
4
2
0
2.30
2.35
2.40
2.45
ENERGY (keV)
SULFUR KαL^n SATELLITES
Na2SO4
NaSCN
n=0
1
2
3
4
5
6

Figure 1

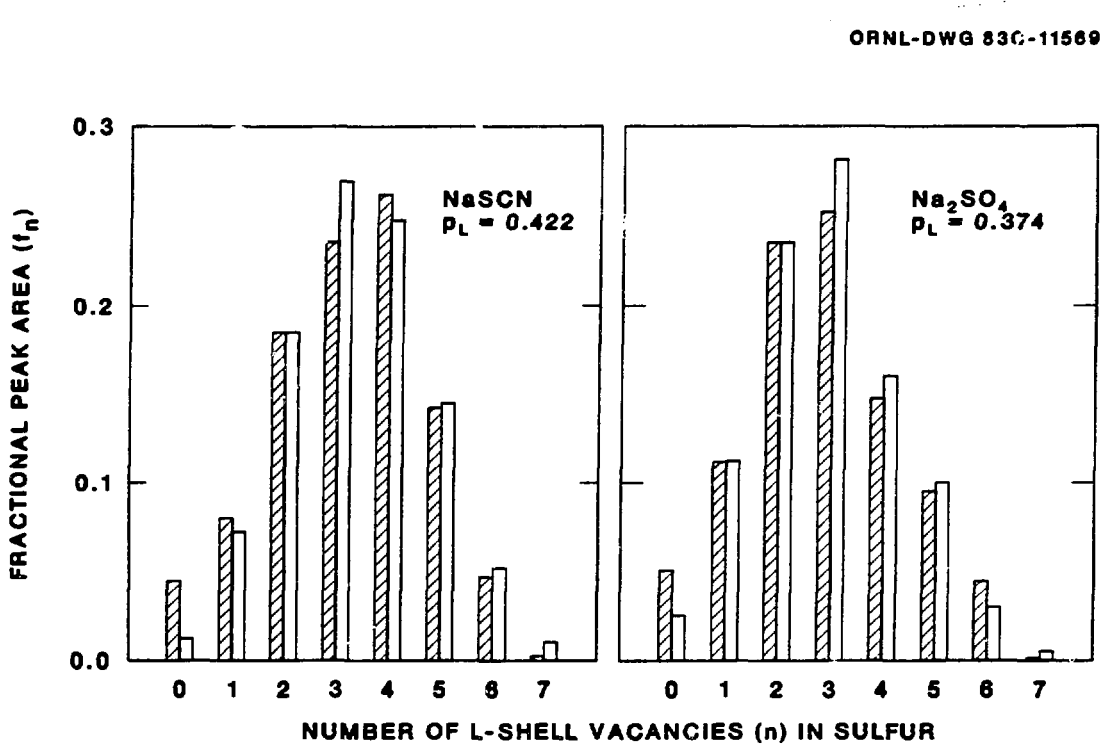
ORNL-DWG 83C-11569
FRACTIONAL PEAK AREA (f_n)
0.3
0.2
0.1
0.0
NaSCN
p_L = 0.422
Na_2SO_4
p_L = 0.374
0 1 2 3 4 5 6 7
0 1 2 3 4 5 6 7
NUMBER OF L-SHELL VACANCIES (n) IN SULFUR

Figure 2

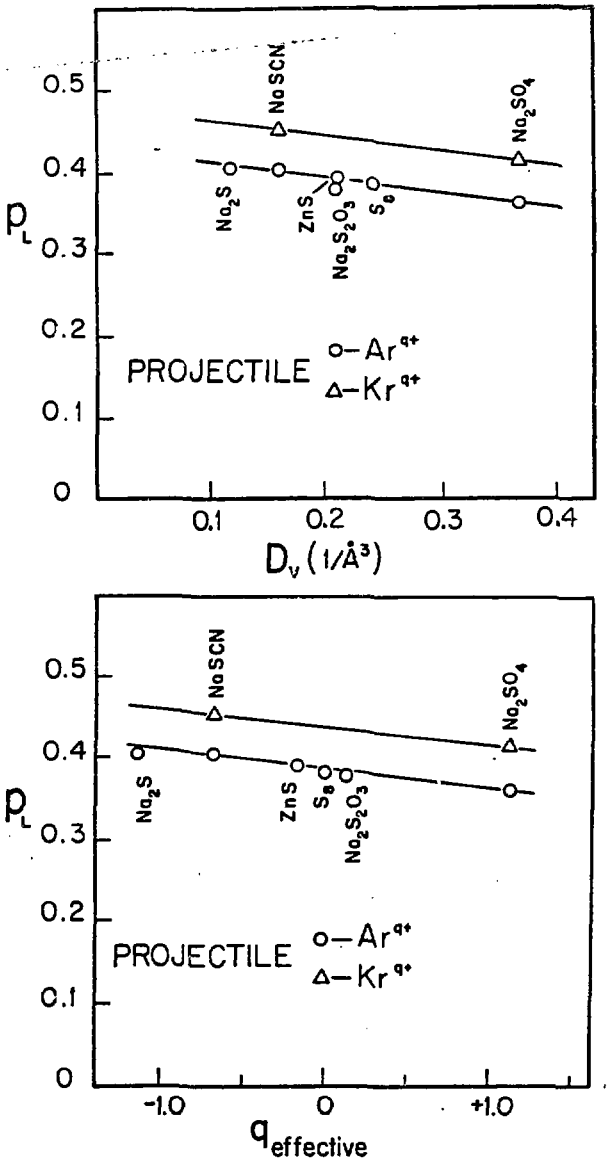
0.5
0.4
0.3
0.2
0.1
0
p_L
NaSCN
Na_2SO_4
Na_2S
ZnS
$Na_2S_2O_3$
S_8
PROJECTILE
o–Ar^{q+}
Δ–Kr^{q+}
0.1
0.2
0.3
0.4
D_v (1/Å^3)
-1.0
0
+1.0
$q_{effective}$

Figure 3

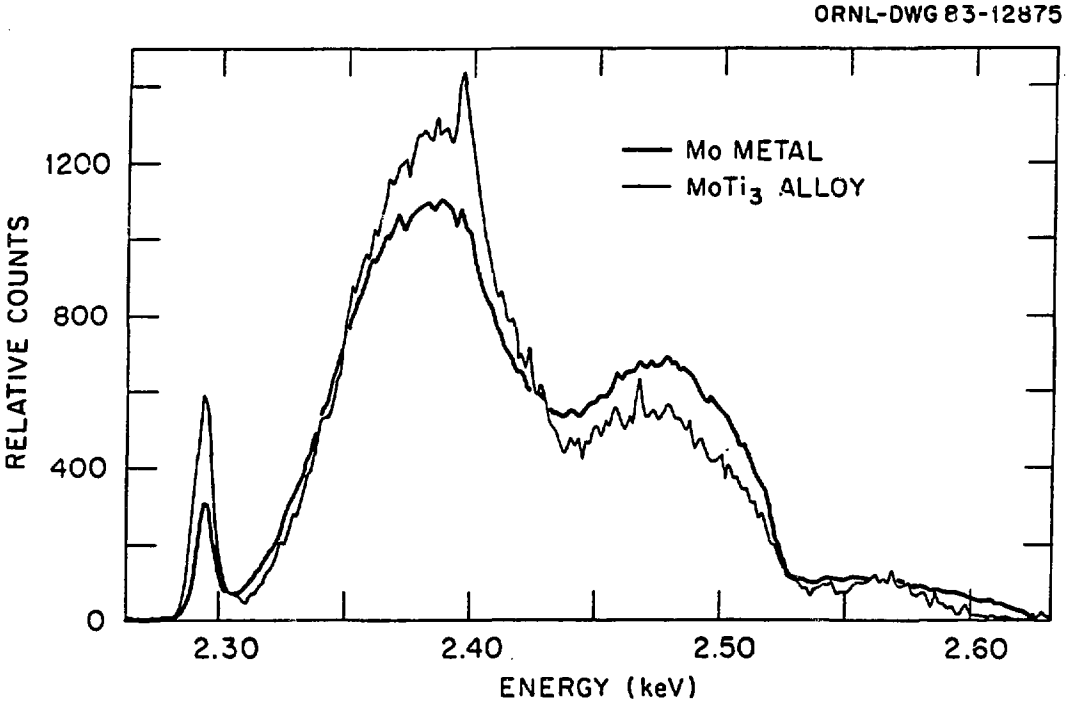
ORNL-DWG 83-12875
Mo METAL
MoTi3 ALLOY
RELATIVE COUNTS
1200
800
400
0
2.30
2.40
2.50
2.60
ENERGY (keV)

Figure 4

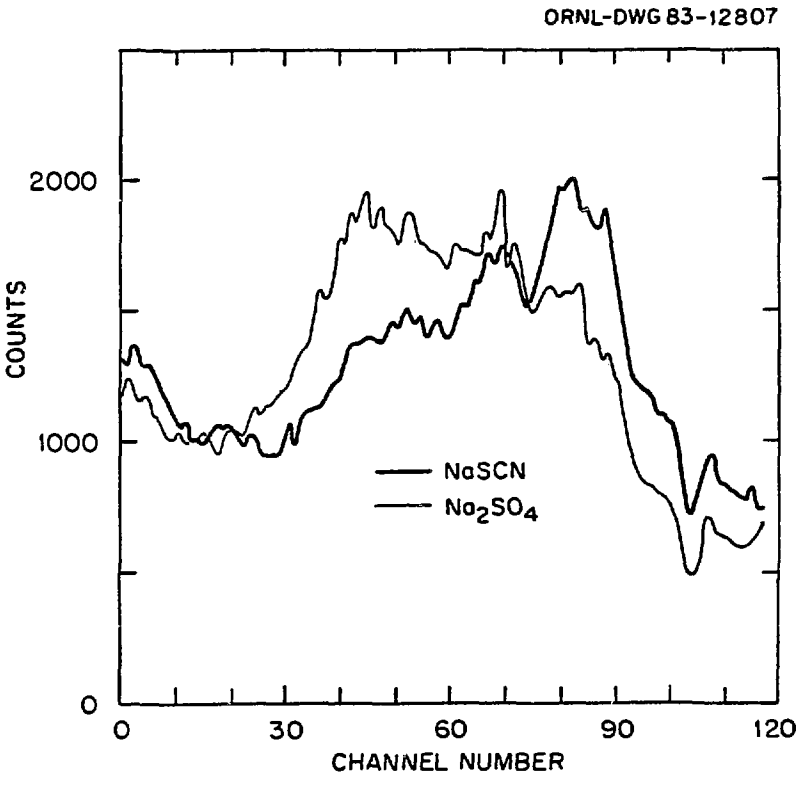
ORNL-DWG 83-12807
2000
1000
0
COUNTS
0
30
60
90
120
CHANNEL NUMBER
NaSCN
Na_2SO_4

Figure 5